Microgravity Q. Vol. 2, No. 3, pp. 141–151, 1992
Printed in Great Britain.

0958-5036/92 $5.00 + 0.00

ON THE STABILITY OF PLANE-PARALLEL ADVECTIVE FLOWS IN LONG HORIZONTAL LAYERS

G. Z. GERSHUNI,[1] P. LAURE,[2] V. M. MYZNIKOV,[3] B. ROUX[4] and E. M. ZHUKHOVITSKY[3]

[1]Department of Theoretical Physics, Perm State University, Bukirev Str., 15, Perm, Russia,
[2]Laboratoire de Mathématiques, UA 168 CNRS, Université de Nice, Parc Valrose, 06034 Nice, France,
[3]Department of Physics, Perm State Pedagogical Institute, K. Marx Str. 24, Perm, Russia and
[4]Institut de Mécanique des Fluides, UM 34 CNRS, 1, rue Honnorat, 13003 Marseille, France

Abstract—Stability of convective motions in a long horizontal cavity differentially heated is studied by means of small perturbation method. We consider either rigid or free upper boundary. In the numerical procedure, we use both the Galerkin and Tau–Chebychev methods. The form of the basis flow allows us to identify three perturbing mechanisms (hydrodynamic, helical wave and Rayleigh modes). Let us note that the last mechanism is directly related to the conducting boundary conditions and does not occur in the adiabatic case. A detailed analysis of the decrement spectrum in terms of Gr has been performed for various Prandtl numbers and allows us to identify the range of Pr in which the different instabilities occur. For small value of Pr ($\mathrm{Pr} < 0.1$), the most critical instability is an hydrodynamic plane mode. For moderate Prandtl number ($\mathrm{Pr} \sim 0.1$), the instability is caused by helical wave mode, while for higher values ($\mathrm{Pr} > 1$) it is an helical "Rayleigh" mode. When the upper boundary is free, we have essentially the same mechanisms. But for strong thermocapillary effects, the hydrodynamic mode does not occur and the two other modes appear earlier in term of Grashof number.

1. INTRODUCTION

The problem of advective liquid flows in layers submitted to horizontal temperature gradients has been the subject of a lot of investigations. Such flows arise in various important technological processes, in particular for production of monocrystals from melts by an horizontal variant of the directional solidification method.

The specific character of advective flows is that vertically directed buoyancy force brings about the uprising of longitudinal pressure gradient causing the horizontal flow, thus the flow and the convective force which generates it are mutually perpendicular. This force affects in some specific way the structure of velocity and temperature fields and therefore the mechanisms of instability have different physical natures.

This paper gives a synthesis of the stability analysis of two types of advective flow in a layer with constant longitudinal temperature gradient applied on horizontal boundaries of high heat conductivity. The first flow type, named Rigid–Rigid (R–R) case, corresponds to the symmetric case of both solid horizontal boundaries. In the second case, named Rigid–Free (R–F), the lower boundary is solid and the upper one is free; then the thermocapillary Marangoni effect is taken into account. The basic states for velocity and temperature, and the governing equations for the disturbances are given in Section 2. This paragraph also presents the two numerical methods used (Galerkin and Tau–Chebychev methods). The former allows us to determine more precisely the origin of the most critical instability, while the latter is easier to use because one can write directly a three-dimensional formulation. In Section 3, the R–R case is discussed. Firstly, the character of different instability mechanisms is studied in detail, and three ways to produce instabilities are identified. Then, we look at linear stability of the parallel advective flow under the action of plane (2D) disturbance and a special limiting type of 3D disturbance (called longitudinal rolls in the sequel). The critical disturbance characteristics are presented and the forms of the new flow patterns are plotted. In the following Section 4, we consider the R–F case. As the general mechanisms are the same, we only focus our attention on the influence of the asymmetric basic state and the thermocapillary forces.

This study deals with the complete range of Prandtl numbers, from small ($\mathrm{Pr} \sim 0.001$) to large ($\mathrm{Pr} \sim 50$) values. It combines and re-analyzes some previous and new results obtained by Perm's school (most of which were not published in English before) and by two French groups.

2. PROBLEM FORMULATION (LINEAR HORIZONTAL TEMPERATURE DISTRIBUTION)

We consider an horizontal fluid layer of infinite extent limited from below and above by parallel planes $x = \pm h$ (coordinate axes are shown in Fig. 1). We assume that the temperature along these two planes changes linearly as a function of (horizontal) z-coordinate

$$T = Az \quad \text{at } x = \pm h, \tag{1}$$

where A is the constant longitudinal temperature gradient.

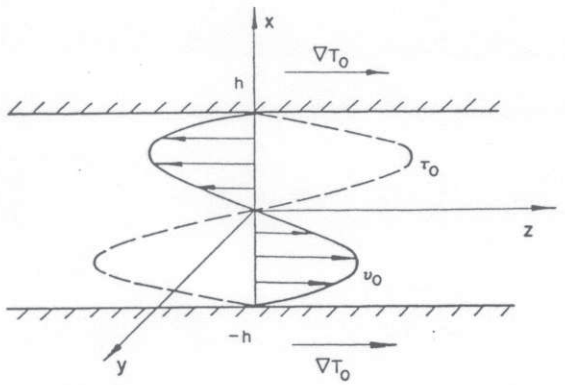

Fig. 1. The coordinate axes. Velocity and temperature profiles in the horizontal layer with both rigid boundaries.

The study of the flows and the analysis of their stability will be carried out on the basis of the free convective equations in the Boussinesq approximation

$$\partial V/\partial t + (V\cdot\nabla V) = -\rho^{-1}\nabla p + \nu\Delta V + g\beta T\gamma,$$
$$\partial T/\partial t + (V\cdot\nabla T) = \kappa\Delta T,$$
$$\nabla\cdot V = 0, \tag{2}$$

where the following symbols are introduced: V, velocity; p, pressure (reference point is hydrostatic corresponding to the average density ρ); T, temperature referred to some arbitrary zero; g, gravity acceleration; γ, unit vector directed vertically upwards; β, ν, κ, coefficients of thermal expansion, kinematic viscosity and heat diffusivity respectively.

The dynamical boundary conditions are the classical no-slip conditions ($V = 0$) on rigid boundary, and zero normal-velocity and prescribed shear stress on "free" boundary. In this last case, a tangential (thermocapillary) force due to temperature dependence on surface tension coefficients $\sigma(T)$ is considered. Then, the balance of viscous and thermocapillary forces gives the relation

$$\rho\nu(\partial V/\partial x)_{x=h} = (\mathrm{d}\sigma/\mathrm{d}T)(\partial T/\partial z)_{x=h}$$

where $(\mathrm{d}\sigma/\mathrm{d}T)$ is assumed to be constant (in most cases, this constant is negative). Here, due to condition (1), $(\partial T/\partial z)_{x=h}$ also is a constant, equal to A.

2.1. Non-dimensionalization, parameters

The Boussinesq equations (2) can be re-formulated in dimensionless form with the following reference quantities: h, h^2/ν, $g\beta Ah^3/\nu$, Ah and $\rho g\beta Ah^2$, respectively for length, time, velocity, temperature and pressure. Then they take the following form

$$\partial V/\partial t + \mathrm{Gr}(V\cdot\nabla V) = -\nabla p + T\gamma + \Delta V,$$
$$\partial T/\partial t + \mathrm{Gr}(V\cdot\nabla T) = \mathrm{Pr}^{-1}\Delta T,$$
$$\nabla\cdot V = 0. \tag{3}$$

These equations contain two dimensionless parameters: the Grashof number (based on the longitudinal temperature gradient and half of the layer thickness) and the Prandtl number

$$\mathrm{Gr} = g\beta Ah^4/(\nu^2); \quad \mathrm{Pr} = \nu/\kappa.$$

2.2. Basic flow

We consider the plane parallel stationary flow, as suggested by Birikh [1]

$$V = [0, 0, v_0(x)]; \quad T = T_0(x, z) = z + f_0(x);$$
$$p = p_0(x, z).$$

The velocity, $v_0(x)$, the temperature, $T_0(x, z)$, and the pressure, $p_0(x, z)$, of this basic flow may be obtained from the general equations (3)

$$\partial p_0/\partial z = v_0'',$$
$$\partial p_0/\partial x = T_0,$$
$$T_0'' = \mathrm{Gr}\,\mathrm{Pr}\,v_0, \tag{4}$$

(here the prime denotes differentiation with respect to x-coordinate).

The thermal boundary conditions (1) simply write: $f_0(\pm 1) = 0$.

2.2.1. Rigid–Rigid case. In the Rigid–Rigid case, the dynamical boundary conditions of no-slip and closed flow lead to

$$v_0(\pm 1) = 0 \quad \text{and} \int_{-1}^{1} v_0\,\mathrm{d}x = 0. \tag{5}$$

The solution of (4), (5) has the form

$$v_0(x) = [x^3 - x]/6,$$
$$T_0(x, z) = z + \mathrm{Gr}\,\mathrm{Pr}\,\tau_0(x), \tag{6}$$

with

$$\tau_0(x) = [3x^5 - 10x^3 + 7x]/360. \tag{7}$$

The velocity profile $v_0(x)$ is presented in Fig. 1; it exhibits two opposing advective flows. The temperature profile $\tau_0(x)$ is described by an odd polynomial of the fifth power (see also Fig. 1). Such profiles may be found experimentally in the middle part of a layer which is sufficiently extended in horizontal directions.

2.2.2. Rigid–Free case. In the Rigid–Free case (with thermocapillary effect), the dynamical boundary conditions write

$$v_0(-1) = 0, \quad \partial v_0/\partial x = -W\,\partial T_0/\partial z \text{ at } x = 1$$
$$\text{and} \int_{-1}^{1} v_0\,\mathrm{d}x = 0 \tag{8}$$

and the solution of (4) and (7) has the form

$$v_0(x) = [(4x^3 - 3x^2 - 6x + 1)$$
$$-3W(3x^2 + 2x - 1)]/24,$$
$$\tau_0(x) = [(4x^5 - 5x^4 - 20x^3 + 10x^2 + 16x - 5)$$
$$-5W(3x^4 + 4x^3 - 6x^2 - 4x + 3)]/480. \tag{9}$$

Here $W = -(\partial\sigma/\partial T)/\rho g\beta h^2$, is a third dimensionless parameter which corresponds to the ratio

between Reynolds-Marangoni number [defined by $\mathrm{Re} = -(\partial\sigma/\partial T)Ah^2/\rho\nu^2$] and Grashof number.

2.3. Disturbances equations

Let us introduce small disturbances of the basic flow and consider the disturbed velocity, temperature and pressure fields

$$V = V_0 + V'; \quad T = T_0 + T'; \quad p = p_0 + p'. \tag{10}$$

where V', T' and p' are small disturbances. After substituting (10) into (3) and linearizing in the vicinity of the basic state, we obtain a system of linear equations for disturbances (dropping the primes of V', T', p')

$$\partial V/\partial t + \mathrm{Gr}(V_0\cdot\nabla V + V\cdot\nabla V_0) = -\nabla p + T\gamma + \Delta V,$$
$$\partial T/\partial t + \mathrm{Gr}(V_0\cdot\nabla T + V\cdot\nabla T_0) = \mathrm{Pr}^{-1}\Delta T,$$
$$\nabla\cdot V = 0. \tag{11}$$

2.3.1. General disturbances. In the general case of spatial normal disturbances, all the variables are proportional to $\exp[-\lambda t + i(k_y y + k_z z)]$ where λ is the characteristic decrement and k_y and k_z are the components of a wave vector along y- and z-axes, respectively.

In the present problem, Squire's theorem does not apply due to the presence of longitudinal temperature gradient. So, the disturbance equations cannot be transformed and reduced to the corresponding plane problem. Nevertheless, we shall discuss in Sections 2.3.2 and 2.3.3 respectively, two limiting cases with plane disturbances ($k_y = 0$) in form of rolls with axes perpendicular to the basic flow, and special spatial disturbances ($k_z = 0$) in form of rolls with axes parallel to the basic flow. In fact, the general study made by Laure [2] shows that most of the disturbances can be decomposed in these two limiting cases.

Let us define the general disturbances ($k_y \neq 0$ and $k_z \neq 0$) as follows

$$V = [u_x(x), u_y(x), u_z(x)]\exp[-\lambda t + i(k_y y + k_z z)],$$
$$p = q(x)\exp[-\lambda t + i(k_y y + k_z z)],$$
$$T = \theta(x)\exp[-\lambda t + i(k_y y + k_z z)]. \tag{12}$$

Then, the governing equations (11) lead to a system of ordinary differential equations for the amplitudes u_x, u_y, u_z, q, θ, which write

$$u_z'' - k^2 u_z - \mathrm{Gr}(ik_z v_0 u_z + v_0' u_x) - ik_z q = -\lambda u_z,$$
$$u_y'' - k^2 u_y - \mathrm{Gr}(ik_z v_0 u_y) - ik_y q = -\lambda u_y,$$
$$u_x'' - k^2 u_x - \mathrm{Gr}(ik_z v_0 u_x) + \theta - q' = -\lambda u_x,$$
$$\theta'' - k^2\theta - \mathrm{Gr}\,\mathrm{Pr}(ik_z v_0\theta + u_x T_0' + u_z) = -\lambda\,\mathrm{Pr}\,\theta,$$
$$i(k_z u_z + k_y u_y) + u_x' = 0. \tag{13}$$

Here, $k^2 = k_y^2 + k_z^2$, and prime denotes differentiation with respect to x.

The amplitude equations (13) with the prescribed boundary conditions define the characteristic decrements $\lambda = \lambda_r + i\lambda_i$ and the associated eigenfunctions. The condition $\lambda_r = 0$ gives the critical value of the Grashof number, Gr_c, as a function of k_y, k_z and Pr; while λ_i gives the frequency of the critical disturbance. We also define the minimal Grashof number as $\mathrm{Gr}_m = \inf_{k_y,k_z}(\mathrm{Gr}_c)$.

2.3.2. Plane disturbances. For plane disturbances ($v_y = 0$, $k_y = 0$, $k_z \neq 0$), the stream function $\psi(x, z, t)$ is introduced

$$\psi(x, z, t) = \phi(x)\exp[-\lambda t + ik_z z],$$

in such a way that

$$u_x = -\partial\phi/\partial z; \quad u_z = \partial\phi/\partial x. \tag{14}$$

Eliminating the pressure, we obtain two amplitude equations for ϕ and θ

$$\phi^{IV} - 2k_z^2\phi'' + k_z^4\phi + ik_z\,\mathrm{Gr}[v_0''\phi - v_0(\phi'' - k_z^2\phi)] - ik_z\theta = -\lambda(\phi'' - k_z^2\phi),$$
$$\theta'' - k^2\theta + ik_z\,\mathrm{Gr}\,\mathrm{Pr}(T_0'\phi - v_0\theta) - \mathrm{Gr}\,\mathrm{Pr}\,\phi' = -\lambda\,\mathrm{Pr}\,\theta, \tag{15}$$

with the following boundary conditions

$$\theta(\pm 1) = 0, \quad \phi(\pm 1) = \phi'(\pm 1) = 0$$

in the R–R case,

$$\theta(\pm 1) = 0, \quad \phi(-1) = \phi'(-1) = \phi(1) = \phi''(1) = 0$$

in the R–F case.

2.3.3. Longitudinal rolls disturbances (L.R.). We consider here a limiting case of 3D spatial disturbance with $k_z = 0$ and $k_y \neq 0$. After eliminating u_y and pressure, the spectral problem for u_x, u_z and θ has the form

$$u_x^{IV} - 2k_y^2 u_x'' + k_y^4 u_x - k_y^2\theta = -\lambda(u_x'' - k_y^2 u_x)$$
$$u_z'' - k_y^2 u_z - \mathrm{Gr}\,v_0' u_x = -\lambda u_z$$
$$\theta'' - k_y^2\theta - \mathrm{Gr}\,\mathrm{Pr}(T_0' u_x + u_z) = -\lambda\,\mathrm{Pr}\,\theta, \tag{16}$$

with boundary conditions

$$u_x(\pm 1) = u_x'(\pm 1) = 0, \quad u_z(\pm 1) = 0, \quad \theta(\pm 1) = 0$$

in the R–R case,

$$u_x(-1) = u_x'(-1) = 0, \quad u_x'(1) = u_x''(1) = 0,$$
$$u_z(-1) = 0, \quad u_z'(1) = 0, \quad \theta(\pm 1) = 0$$

in the R–F case.

Let us remark that for this kind of disturbances the velocity component u_z is not equal to zero. Consequently, the trajectory of a fluid particle is helical.

2.4. Numerical methods

2.4.1. Galerkin method and selection of basic functions. According to the previous works of Gershuni *et al.* [3, 4] and Myznikov [10, 23], we use a Galerkin method in order to approximate the solution of the spectral problems (15) and (16).

For plane disturbances (15) the selected basic functions are the eigenfunctions of two uncoupled limiting problems at Gr = 0. For the stream function amplitude ϕ, one gets

$$\phi_n^{IV} - 2k_z^2\phi_n'' + k_z^4\phi_n = -\mu_n(\phi_n'' - k_z^2\phi_n) \quad (17)$$

with the dynamical boundary conditions

$$\phi_n(\pm 1) = \phi_n'(\pm 1) = 0; \quad n = 0, 1, 2, \ldots$$

in the R–R case, and

$$\phi_n(-1) = \phi_n'(-1) = \phi_n(1) = \phi_n''(1) = 0;$$

$n = 0, 1, 2, \ldots$, in the R–F case.

For the temperature amplitude θ, we have

$$\theta_n'' - k_z^2\theta_n = -\nu_n \mathrm{Pr}\theta_n \quad (18)$$

with the thermal boundary conditions: $\theta_n(\pm 1) = 0$; $n = 0, 1, 2, \ldots$.

These spectral problems give the disturbance spectra for the velocity and the temperature in motionless liquid layer (for Gr = 0). Decrements μ_n and ν_n are real and positive (disturbances of velocity and temperature in motionless liquid layer decay monotonically). Up to 40 basic functions for each expansion $\phi(x)$ and $\theta(x)$ are used. A "good" accuracy is assumed to be reached when solution of spectral problems (15) and (16) does not change by more than 1%. The numerical procedure uses the scheme proposed by Birikh and Rudakov [5].

For L.R. disturbances (16), u_x satisfies the same boundary conditions as ϕ, and thus the basic set (17) is applied with the substitution of k_y instead of k_z. For θ, we also substitute k_y instead of k_z in the basic set (18). For u_z, we use the system of basic functions satisfying

$$u_{zn}'' - k_y^2 u_{zn} = -\chi_n u_{zn} \quad (19)$$

with the boundary conditions: $u_{zn}(\pm 1) = 0$, $n = 0, 1, 2, \ldots$, in the R–R case. Up to 80 basic functions are employed to approximate the amplitudes u_x, θ and u_z.

Following the spectrum classification given by Gershuni and Zhukhovitsky [6] and Gershuni *et al.* [7], the eigenvalues will be labelled as "isothermal" (and presented as dashed curves in the figures) or "non-isothermal" (solid lines), depending if they originate either from momentum equation ("hydrodynamic" type) or energy equation ("thermal" type), respectively. This identification can be made conveniently since for small Gr the two equations become only weakly coupled. For plane disturbances ($k_y = 0$), μ and ν levels will be used on the figures corresponding to ϕ and θ, while the L.R. disturbances ($k_z = 0$) a third level, χ, corresponding to u_z will be employed.

2.4.2. Tau–Chebyshev method. Tau technique is a well known variant of Galerkin technique in which the basic functions do not verify automatically the boundary conditions [8]. Instead of that, specific equations describing boundary conditions have to be used. Here, Chebyshev polynomials have been used for all the variables of the full system (13). This method is popular due to the high accuracy of Chebyshev approximation, and due to the simplicity to represent: (i) boundary conditions at $x = \pm 1$, (ii) the basic flow in terms of Chebyshev expansion, and (iii) the convolution product between two series with known and unknown Chebyshev coefficients. A detailed description can be found in previous papers [8, 9] for eigenvalues analysis.

3. FLOW MOTION IN A LAYER WITH UPPER AND LOWER RIGID BOUNDARIES (R–R CASE)

3.1. Expected mechanisms of instability

Before presenting quantitative results of the spectral problems (15) and (16) we review expected physical mechanisms of instability. As shown in Fig. 1, the basic velocity profile (6) possesses an inflection point occurring in the centre of the layer section $x = 0$. Due to the occurrence of the inflection point the basic flow must display inviscid instability mode. This mode is related to the formation of stationary vortices on the frontier of the two opposing flows.

Moreover, Fig. 1 shows that the basic temperature profile (6) has two zones of potentially unstable stratification near the upper and lower horizontal boundaries. In these zones the onset of (Rayleigh) "stratificational" instability caused by heating from below becomes possible. However, this instability cannot appear at the equilibrium state (Gr = 0). For higher value of Gr, it grows to the opposite direction of the basic flow.

Finally, as the central part of the liquid layer is stratificated in potentially stable manner, the generation of disturbances as inner waves of gravitational type may be expected. At Gr = 0 [see equation (6)], this kind of disturbance is damped. Generally speaking, when the liquid is moving (Gr > 0), their appearance is expected, due to the interaction with the basic flow.

The calculations indicate that these three mentioned mechanisms occur in delimited intervals of Prandtl number. But the first and the third mechanisms developing in the zone of stable stratification disappear when Pr increases.

3.2. Plane hydrodynamic modes

We start with the discussion of the results concerning purely hydrodynamic (inviscid) instability mode. Figure 2 presents an example of decrements spectrum of plane disturbances for Pr = 0.01. Figure 2(a) shows the real part of characteristic decrements, λ_r, and Fig. 2(b) the imaginary parts, λ_i. Dashed curves depict branches corresponding to the disturbances of the "hydrodynamic" type, solid curves correspond to "thermal" branches (see spectrum classification

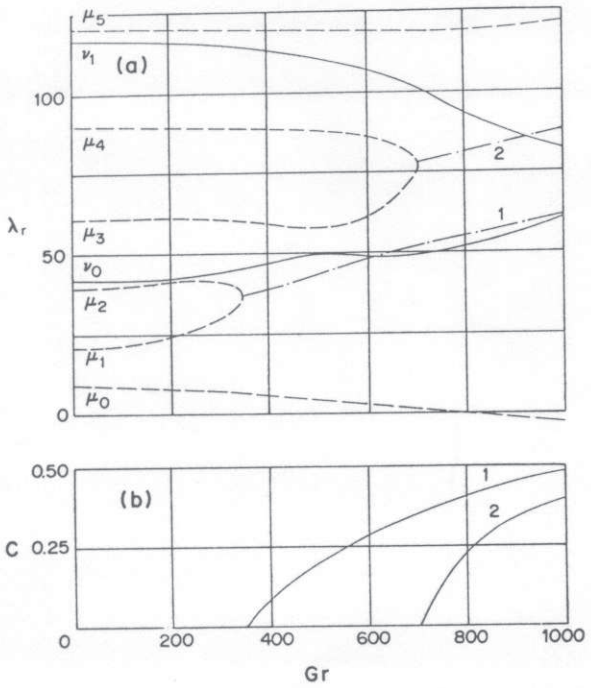

Fig. 2. (a) Real part of the lowest levels of the decrements spectrum versus Grashof number for hydrodynamic instability (Pr = 0.1; $k_z = 1.3$). (b) Phase velocity modulus.

detailed by [6, 7]). It is evident that for small values of Gr in conformity with the general theory (described in these previous works) decrements are real and positive, i.e. all disturbances decay monotonically.

The lowest spectrum level of "hydrodynamic" type ("μ_0" level) vanishes for some value of Grashof number which corresponds to the emergence of a monotonous instability. Other spectrum levels do not cause instability. As Gr increases, some levels "coalesce" pairwise (pairs of complex-conjugated decrements are formed). In the coalescence points, the pairs of decaying disturbances develop as waves differing by the sign of the phase velocity. This phase velocity, c, expressed in units of the maximum velocity of the basic flow is directly connected to the imaginary parts of the decrements

$$c = \frac{9\sqrt{3}}{k_z \mathrm{Gr}} |\lambda_i|. \tag{20}$$

It is presented in Fig. 2(b) as a function of Gr.

The neutral curves, $\mathrm{Gr}_c(k_z)$, for different values of Prandtl number have a minimum for k_z bounded by 1.2 and 1.3. It is evident that the increase of Pr leads to a quick stabilization of this hydrodynamic mode, because it is localized in the zone of stable stratification.

The form of characteristic disturbances leading to instability of the basic flow can be determined from the eigenfunctions of the system (15). The flow patterns are not represented here. As in the vertical layer [6], this instability leads to the formation of a vortex system, periodic in the z-direction, located on the frontier of two opposite flows.

3.3. Plane Rayleigh mode

Now we discuss the stratificational (Rayleigh) instability mode. The calculations indicate that this mode is important in the range of moderate and large Prandtl numbers and exists in both classes of plane and L.R. disturbances.

Figure 3 shows the decrement spectrum of plane disturbances for Pr = 10 and $k_z = 4$. It is obvious that for comparatively small Grashof numbers coalescence of real levels occurs with the formation of complex-conjugated pairs. The levels of thermal type are concentrated in the lowest part of the spectrum. When increasing Grashof number, oscillating flow instability arises due to the "mixture" of ν_0- and ν_1-levels. In the critical point, a pair of growing disturbances appears as travelling waves extending in the two opposing basic flows. One of the waves, possessing negative phase velocity, spreads along the "upper" warmer flow (drift of convective Rayleigh cells originated in the "upper" unstable stratificated zone). Another wave, with positive phase velocity, drifts to the right in the "lower" colder (unstably stratificated) zone. From the point of view of stability, these two waves are equivalent.

The family of neutral curves $\mathrm{Gr}_c(k_z)$ for different Pr ranging from 1.5 to 50 has a minimum for k_z close to 4. That indicates the relatively short wave character of this instability. When increasing Pr, the

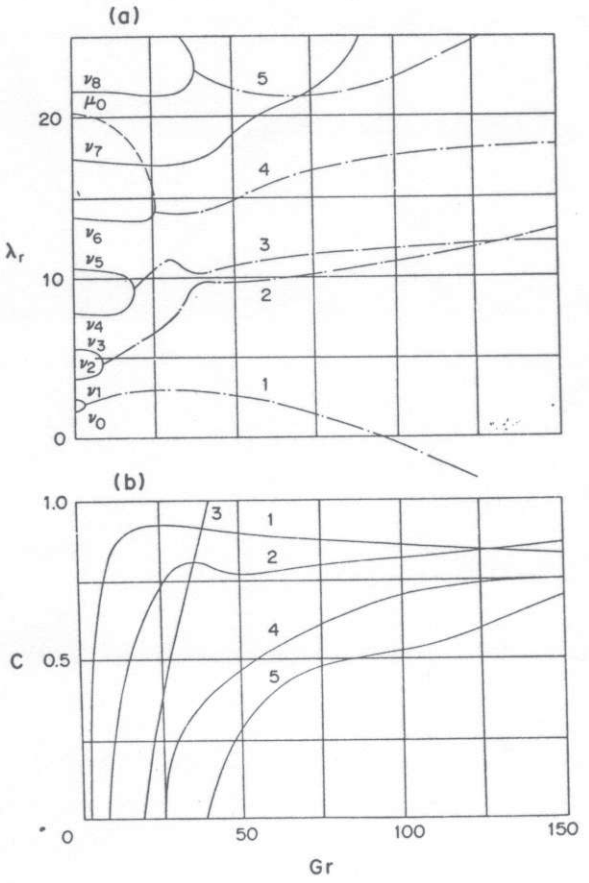

Fig. 3. (a) Real part of the lowest level of the decrements spectrum versus Grashof number for plane Rayleigh instability (Pr = 10; $k_z = 4$). (b) Phase velocity modulus.

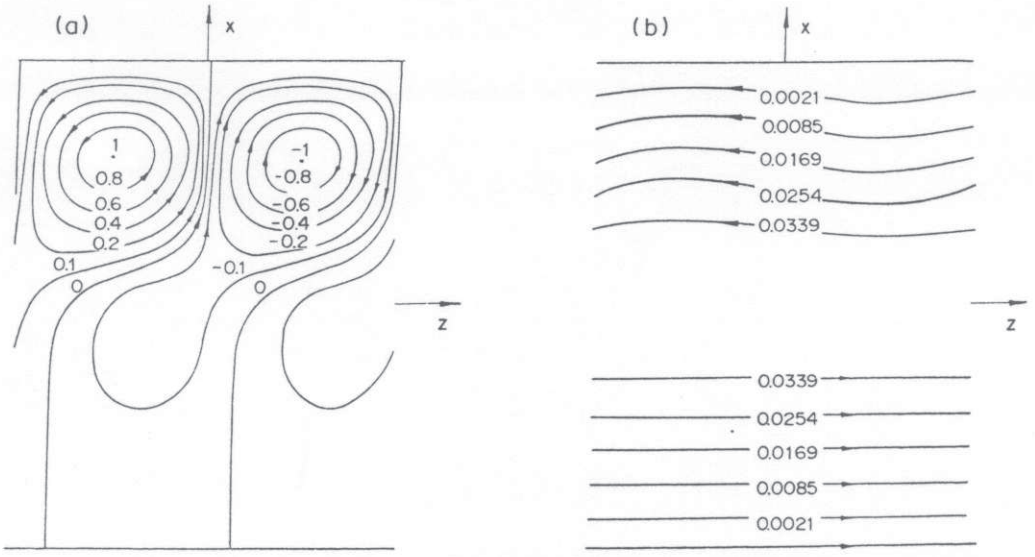

Fig. 4. The stream function isolines for plane Rayleigh modes (Pr = 10; Gr = 100; $k_z = 4$). (a) Disturbances. (b) Secondary flow.

minimal Grashof number decreases monotonously and exhibits an asymptotic dependence $Gr_m = 964/Pr$. Thus the relevant critical parameter is the Rayleigh number, $Ra_m = Gr_m Pr$, indicating the stratificational nature of the instability. The phase velocity of the critical disturbances weakly depends on Prandtl number; c_m increases monotonously from 0.67 to 0.86 when Pr increases from 0.6 to 50.

The plane Rayleigh modes are characterized by disturbances in cell structure which are practically localized in upper or lower parts of the layer. Thus, opposing waves appear as the result of superposition of these disturbances with the basic flow. Figure 4 presents stream function isolines for the "upper" wave with negative phase velocity (the "lower" flow is practically not disturbed). Figure 5 shows the corresponding temperature isolines. We have the opposite situation for the wave with positive phase velocity.

3.4. *L.R. Rayleigh mode (S.L.R.)*

Now we discuss L.R. Rayleigh modes which are shown to be more dangerous than plane ones in the whole range of Prandtl numbers. The derivatives v_0' and T_0' are even functions of x, so the spectral problem (16) admits solutions of a certain symmetry with respect to x. Thus, disturbances spectra and stability limits can be found for even and odd modes.

One example of spectrum including levels of even and odd types is shown in Fig. 6. It is obvious from the spectrum structure that the interaction of levels of identical parity takes place. Two critical points linked

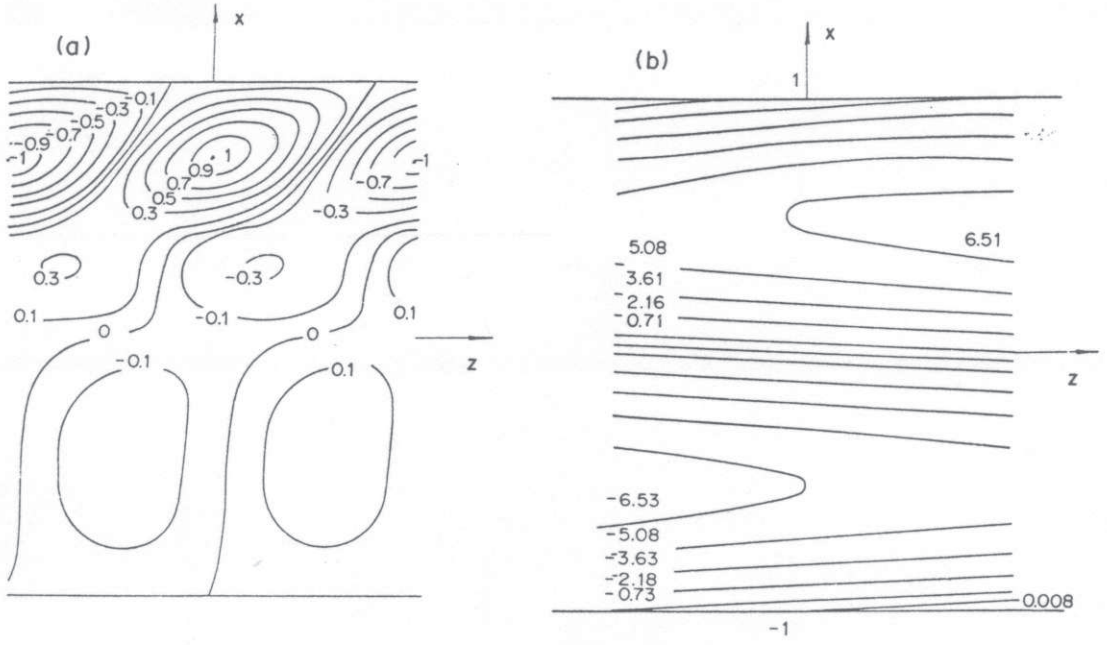

Fig. 5. The isotherms for plane Rayleigh modes (Pr = 10; Gr = 100; $k_z = 4$). (a) Disturbances. (b) Secondary flow.

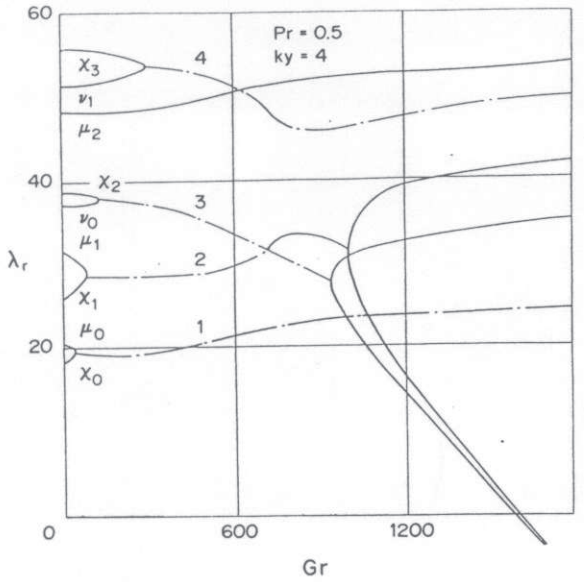

Fig. 6. Real parts of the lowest levels of decrements spectrum for S.R.L. Rayleigh instability ($Pr = 0.5$; $k_y = 4$).

with the onset of instability of the monotonous type exist. In this example, the lowest instability level (even) appears due to the mixture of the ν_0 thermal branch and the χ_2 hydrodynamic branch. The second instability level (odd) emerges from the mixture of the χ_1 and μ_1 branches. The monotonous character of the instability and the presence of two, close, critical points remains for other values of Pr and k_y. Thus, we prefer to use the term stationary longitudinal rolls (S.L.R.) for this kind of instability.

Neutral curves for even and odd S.L.R. modes have a minimum for k_y close to 4. For small Pr ($Pr < 0.03$) the odd mode is the most dangerous; but as Pr increases, the situation changes to the opposite. Furthermore it appears that a shift of parity of the most dangerous mode occurs once more when $Pr = 2.7$. For large Pr, asymptotic laws $Gr_m = a/Pr$ (characteristic of Rayleigh mechanism) hold for both even and odd modes, with $a = 886$ for even mode and $a = 879$ for odd mode. It may be noted that in the limit case $Pr \to \infty$, the marginal stability may be determined by means of a simplified asymptotic boundary problem [4].

The structure of even and odd disturbances of S.L.R. type, in the (x, y)-plane, are plotted in Fig. 7. For even disturbances, the flow pattern is a system of two main vortices with similar circulation direction situated in the zones of unstable stratification, and there is between them a weak vortex of opposite circulation [Fig. 7(b)]. Odd disturbances consist of two vortices of opposite circulation [Fig. 7(a)].

3.5. Oscillating wave mode (O.L.R.)

We present results referring to the latter of the mentioned instability mechanisms, i.e. linked with the generation of growing inner gravitational waves in the zone of stable temperature stratification. Disturbances describing these mechanisms belong to the class of even L.R. modes [spectral problem (16)]. In contrast to L.R. Rayleigh modes possessing monotonous character, the critical disturbances develop in this case as a pair of travelling waves in the y-direction. Then, this instability is called oscillating longitudinal roll in the sequel (O.L.R.). It may be also noted that such inner waves come to be a long wave and exist only in the interval of small Prandtl numbers. Solution of (16) was carried out by Myznikov [10] with the method described above and with a Galerkin procedure involving up to 80 basis functions.

Figure 8 gives an example of spectrum which makes evident that the O.L.R. mode for $Pr = 0.25$ and $k_y = 1.6$ exists in a bounded range of Rayleigh numbers and is formed by a mixture of "lower" even

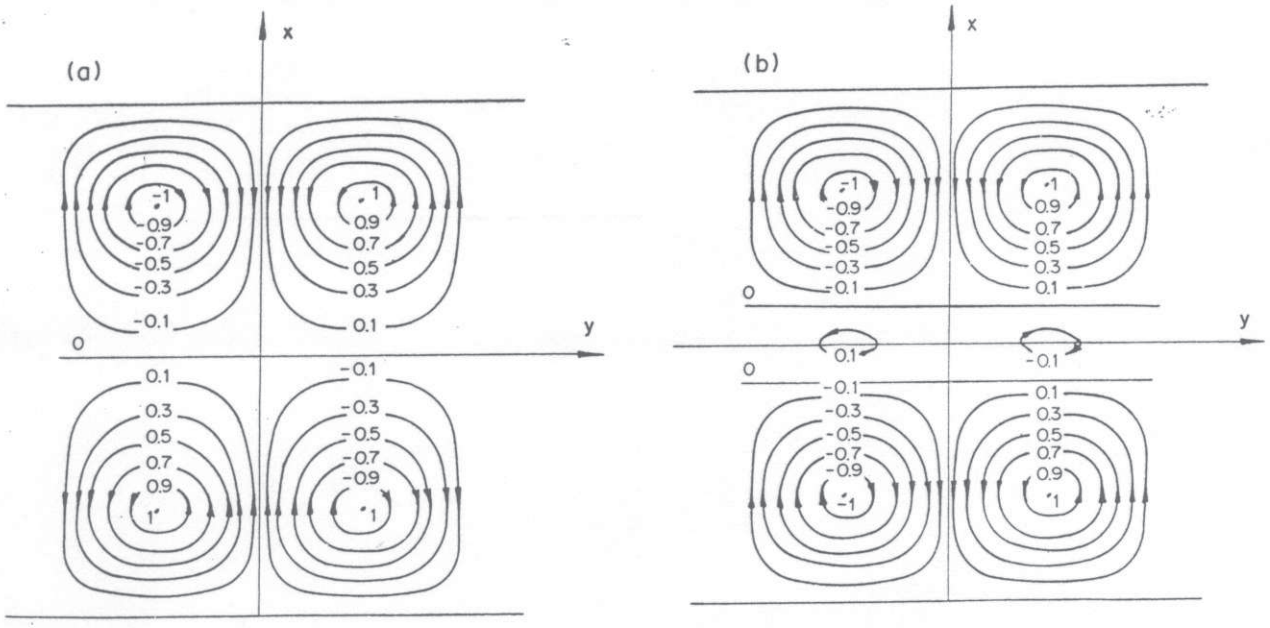

Fig. 7. The stream function isolines in $(x-y)$ plane for even S.L.R. Rayleigh mode (a) and odd one (b).

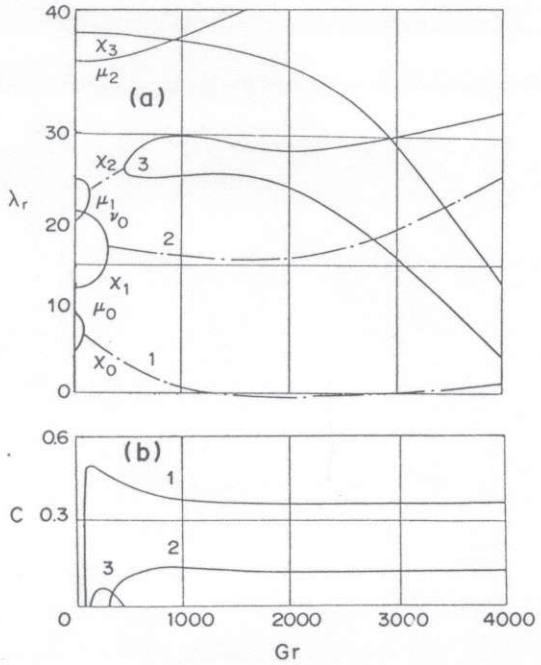

Fig. 8. (a) Real parts of the lowest levels of decrements spectrum for O.L.R. instability (Pr = 0.25; $k_y = 1.6$). (b) The imaginary ones.

hydrodynamic levels, μ_0 and χ_0. Critical Rayleigh number is plotted in Fig. 9. The O.L.R. mode exists in the range of small values of Prandtl number (Pr < 0.456) with $k_y < 2.5$. The results agree well with those given by [11–13].

3.6. Conclusions

Figure 10 summarizes the stability results obtained for all the critical modes discussed in this paragraph. For small Prandtl numbers ($0 \leqslant \mathrm{Pr} < 0.14$) the most dangerous is the plane monotonous hydrodynamic

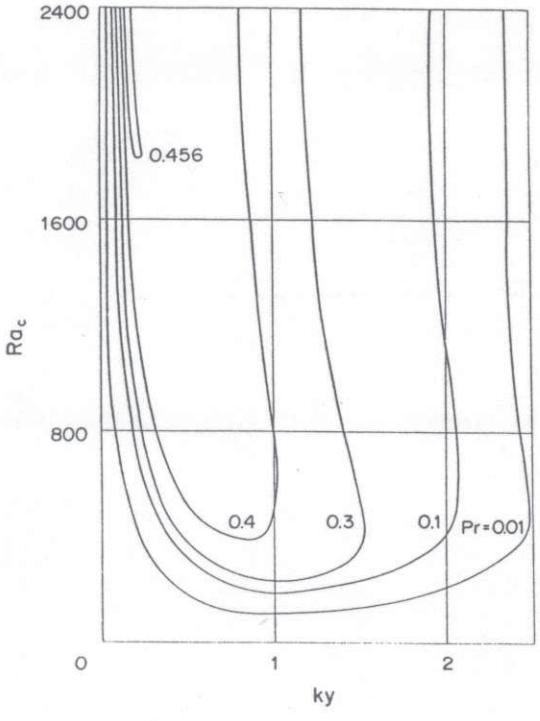

Fig. 9. Critical Rayleigh numbers for O.L.R. instability.

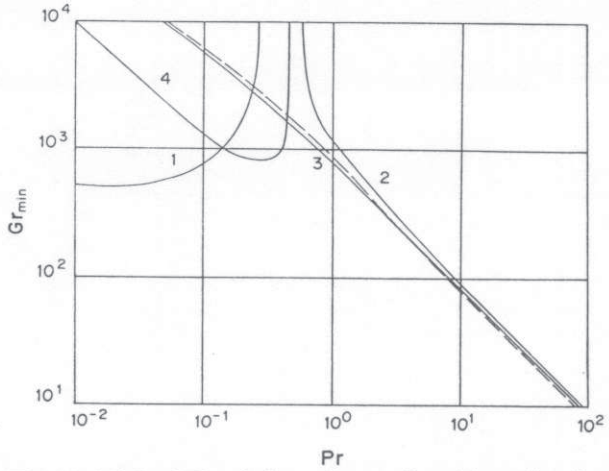

Fig. 10. Minimal Grashof number vs Prandtl number for various instability modes: 1—plane hydrodynamic mode; 2—plane Rayleigh mode; 3—even (solid curve) and odd (dashed curve) S.R.L. Rayleigh modes; 4—O.L.R. mode.

mode. In a narrow range of Prandtl numbers ($0.14 < \mathrm{Pr} < 0.44$) instability is caused by O.L.R. mode. For Pr ~ 0.44 the instability is transferred by S.R.L. monotonous mode of the Rayleigh type which remains the most dangerous up to extremely large Pr.

An experimental investigation of the advective flow of ethanol (Pr = 16.1) in shallow cavity was carried out by Berdnikov and Zabrodin [14]. The crisis of the basic flow was observed in the interval $54 \leqslant \mathrm{Gr} \leqslant 72$ for k_{ym} varying from 2.9 to 4.3; this is connected to the onset of S.R.L. disturbances. The theory predicts that instability due to S.R.L. odd mode arises when $\mathrm{Gr_m} = 55$ and $k_{ym} \approx 4$. The agreement between theory and experiment may be regarded as satisfactory.

Calculation of stability boundary for plane hydrodynamic modes in the case of a conducting fluid subjected to a transverse magnetic field has been done by Aristov and Pichugin [15]. As one would expect, magneto-hydrodynamic (MHD) interaction causes strong flow stabilization.

4. FLOW MOTION IN A LAYER WITH RIGID LOWER AND FREE UPPER BOUNDARIES

We consider now an asymmetric case of a horizontal layer with a rigid lower surface and a free upper boundary subjected to thermocapillary effect. The upper boundary is assumed to be plane and the temperature along the horizontal boundaries is linear (the boundary conditions $\tau_0(1) = 0$ for the base flow and $\theta(1) = 0$ for the perturbation may be organized by means of an intensive heat transfer on the upper free surface). The no-slip condition is assumed on the lower boundary. The basic dimensionless velocity and temperature profiles are given by the expressions (8), in terms of W which characterizes the ratio between thermocapillary and buoyancy forces (W can also be written as $W = \mathrm{Re/Gr}$). These basic profiles are decomposed into two terms, the first one is due to buoyant effects, the second one (multiplied by W) is the contribution of thermocapillary effects. The

thermogravitational flow component prevails if $|W| \ll 1$, while thermocapillary effect is dominant when $|W| \gg 1$. Examples of basic velocity and temperature profiles are presented in Fig. 11.

When $0 \leqslant W \leqslant 1$, the velocity distribution has an inflection point. The position of this point moves toward the upper boundary when W increases from zero to one, and the inflection point disappears when $W > 1$. As in the R–R cases, the temperature profiles display two zones of unstable stratification near the boundaries and one zone of stable stratification in the middle part of the layer. The thickness of these three layers and the vertical temperature distribution are functions of the parameter W. The same instability mechanisms described in the previous paragraph are expected to occur. The main difference consists in the asymmetry of the basic profiles of $v_0(x)$ and $\tau_0(x)$ given by the equations (8). Some computations already made by Myznikov [16–18] and Ben Hadid *et al.* [19] are analysed here with some new results showing the influence of W on the three dimensional instabilities.

4.1. Plane hydrodynamic modes

As in the R–R case, the plane hydrodynamic mode causes the onset of instability in the range of small Prandtl numbers. In particular, Fig. 14(a) shows that the increase of Prandtl number from 0.01 to 0.15 causes a strong stabilization for $W = 0.1$ (see also results by Ben Hadid *et al.* [19]). But, as a consequence of profile asymmetry [6] the plane hydrodynamic mode is no longer monotonous. It develops as a vortex system, z-periodic, drifting in the same direction than the "upper" flow. This instability is brought about by the lowest hydrodynamic level μ_0. Calculations indicate that phase velocity is negative (resp. positive) for W greater (resp. smaller) than $-1/3$. At $W = -1/3$, the velocity profile is symmetric and as noted above, the critical eigenvalue λ is equal to 0. The hydrodynamic mode presents a relatively long wave character. The main result is that increasing the absolute value of W causes a strong stabilization. As noted by Laure and Roux [24] this effect could be related to the displacement of the inflection point when W changes. Figure 12 shows that the full

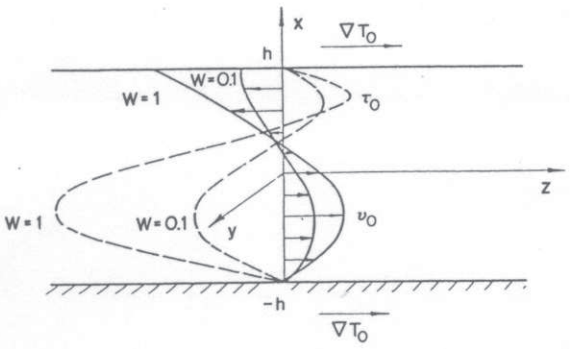

Fig. 11. Examples of basic flow profiles in the layer with free upper boundary.

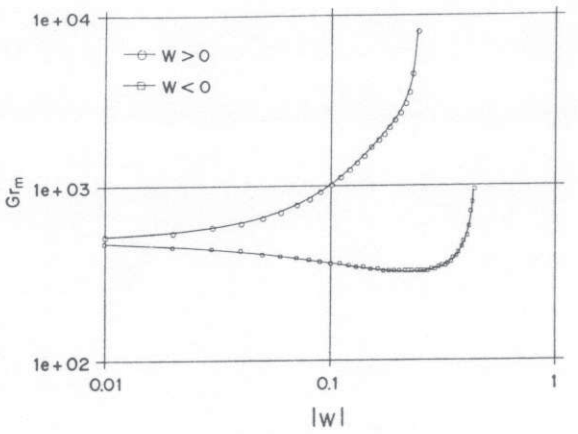

Fig. 12. Stabilization of hydrodynamic mode due to increase of $|W|$ at $\mathrm{Pr} = 0.01$.

stabilization is reached at $W = 0.27$ and $W = -0.5$ for $\mathrm{Pr} = 0.01$.

4.2. Plane Rayleigh modes

The most dangerous mode of two plane Rayleigh modes correspond to the one with positive phase velocity and it is linked to with the lower flow. This result is illustrated in Fig. 13, where the relative positions of curves $\mathrm{Gr_m(Pr)}$ for all Rayleigh modes are plotted for fixed $W = 0.1$. For large Prandtl numbers the critical Grashof number satisfy the asymptotic relation $\mathrm{Gr_m} = a/\mathrm{Pr}$ where the coefficient a, for the most dangerous mode, is respectively equal to 363.8, 215.4 and 198.1 for $W = 0.1$, 1 and 10.

4.3. S.L.R. Rayleigh modes

The critical mode of the L.R. Rayleigh disturbances is also arising in the lower unstable zone (Fig. 13) (it may be emphasized that L.R. modes in the discussed case do not possess definite parity). For large Prandtl numbers the usual asymptotic law, $\mathrm{Gr_m} = a/\mathrm{Pr}$, is obtained where a takes respectively the values 286, 154 and 51 for $W = 0.1$, 1 and 10. The critical wave number k_{ym} is close to 3 and slightly

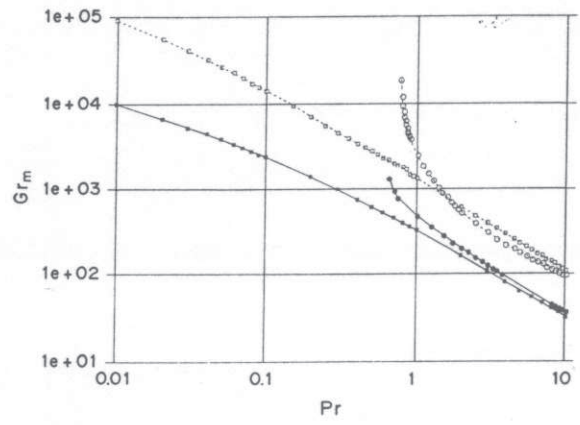

Fig. 13. The neutral curves for Rayleigh instabilities ($W = 0.1$): plane mode in the upper flow (○, dashed line); plane mode in the lower flow (○, solid line); S.R.L. mode in the upper flow (□, dashed line); S.R.L. mode in the lower flow (□, solid line).

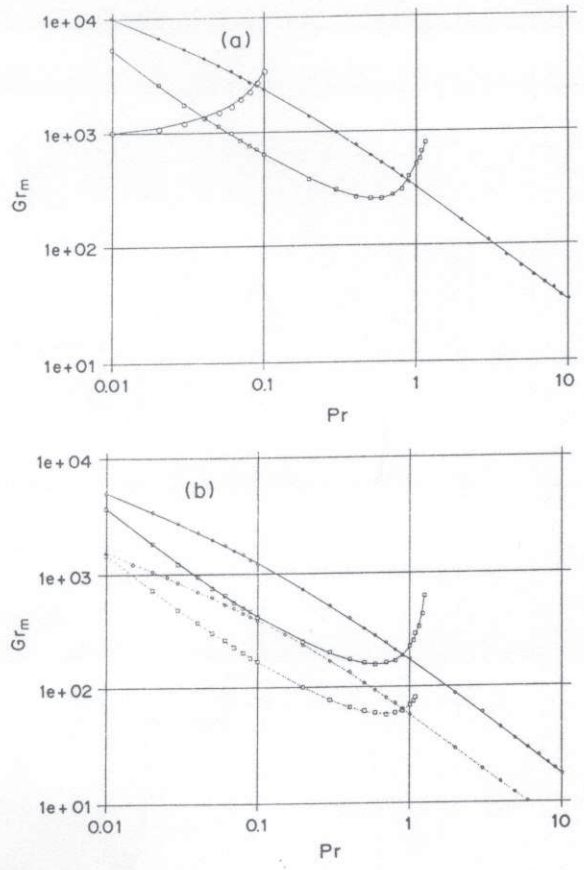

Fig. 14. (a) Minimal Grashof number vs Prandtl number for $W = 0.1$. (b) Minimal Grashof number for $W = 1$ (solid line) and $W = 10$ (dashed line). plane hydrodynamic mode (○); 3D-oscillating mode (□); S.R.L. Rayleigh mode (◇).

changes with Pr. One gets that this mode is monotonous (S.L.R.) and becomes more critical as the thermocapillary forces increase.

4.4. 3D-oscillating mode

This type of instability due to the central stratification have been already studied for both adiabatic and conducting conditions [2, 20, 21] for $W = 0$. In the present paper, we focus on the influence of positive W on this instability. Let us note that in this case k_z is no longer null, and it remains small with respect to k_y ($k_z \sim 0.1k_y$, for $W = 0$) and tends to zero as $|W|$ increases. This mode mainly occurs for moderate Prandtl number ($Pr < 1.5$ in the conducting case). We show that this mode becomes more unstable as the (positive) Marangoni numbers is increased. Nevertheless, this kind of instability is stablized as Pr increases.

4.5. Discussion and conclusion

Summary results referring to the most dangerous disturbances in the layer with a free upper boundary is presented in Fig. 14. When $W = 0.1$ (i.e. when thermogravitational flow component prevails), the crisis is caused by either plane hydrodynamic mode ($Pr < 0.045$), or 3D-oscillating mode ($0.045 \leqslant Pr \leqslant 0.85$) or S.R.L. Rayleigh one ($Pr > 0.85$). For higher values of W, the hydrodynamic mode disappears, and, when $W = 1$ and 10, the most dangerous instability is either 3D-oscillating mode (for $Pr < 1$) or "lower" S.L.R. Rayleigh mode (for $Pr > 1$).

These data confirm that, in the range of moderate and large Pr, the instability is caused by Rayleigh mode (due to the presence of unstable zones on the temperature profile). Naturally this mode does not exist in the case of absence of unstable stratification zones, like in the case of a layer with horizontal insulated boundaries [22] where only hydrodynamic and O.L.R. modes occur in the range of small Pr.

In conclusion, it may be noted that although the Marangoni force is taken into account on the free surface, specific thermocapillary instability mode does not manifest itself. It is connected with the fact that temperature of free surface is given and temperature disturbance is absent [see boundary conditions (7)]. Naturally in case of more "slight" conditions thermocapillary instability develops, as noted by Smith and Davis [25] and Smith [26].

REFERENCES

1. R. V. Birikh, On thermocapillary convection in a horizontal layer of liquid. *J. Appl. Mech. Tech. Phys.*, No. 3, p. 67 (1966).
2. P. Laure, Study of convective motion in a rectangular cavity with horizontal temperature gradient. *J. Mécan. Théor. Appl.* **6,** 351–382 (1987).
3. G. Z. Gershuni, E. M. Zhukhovitsky and V. M. Myznikov, On stability of a plane-parallel convective flow in horizontal layer. *J. appl. Mech. Tech. Phys.*, No. 1, p. 95 (1974).
4. G. Z. Gershuni, E. M. Zhukhovitsky and V. M. Myznikov, Stability of a plane-parallel convective flow in horizontal fluid layer with respect to spatial disturbances. *J. appl. Mech. Tech. Phys.*, No. 5, p. 145 (1974).
5. R. V. Birikh and R. N. Rudakov, Application of orthogonalization technique in step-by-step integrating in reference to stability of convective flows study. In *Hydrodynamics*, No. 5, p. 149. State Univ., Perm (1974).
6. G. Z. Gershuni and E. M. Zhukhovitsky, *Convective Stability of Incompressible Fluid.* Nauka, Moscow. Translated: *Convective Stability of Incompressible Fluid.* Wiley, New York.
7. G. Z. Gershuni, E. M. Zhukhovitsky and A. A. Nepomnyashchy, *Stability of Convective Flows.* Nauka, Moscow (1989).
8. S. A. Orszag, Accurate solution of Orr-Sommerfeld stability equation. *J. Fluid Mech.* **50,** 689–703 (1971).
9. K. I. Babenko, *Foundation of Numerical Analysis.* Nauka, Moscow (1986).
10. V. M. Myznikov, On helical oscillatory instability of a plane-parallel advective flow. *Convective Flows. Perm Pedagog. Inst.*, p. 28 (1989).
11. H. P. Kuo, S. A. Korpela, A. Chait and P. S. Marcus, Stability of natural convection in a shallow cavity. *8th Heat Transf. Conf.*, San Francisco, Vol. 3, p. 1539 (1986).
12. P. Laure and B. Roux, Synthèse des résultats obtenus par l'étude de stability des mouvements de convection dans une cavité horizontale de grande extension. *C.r. Acad. Sci. Paris* **305,** 1137-1143 (1987).
13. D. S. Pavlovsky, Solution of convective stability problems of multicomponent liquids. Preprint No. 416, Inst. Prob. Mech. U.S.S.R. Acad. Sci. (1989).
14. V. S. Berdnikov and A. G. Zabrodin, Experimental investigation of thermogravitational and

gravitational-capillary convection structure with horizontal directed crystallization model. In *Thermophysical Processes in Substances Crystallization*. Novosibirsk: Inst. Thermophysics Sib. Branch, U.S.S.R. Acad. Sci., p. 67 (1987).
15. S. N. Aristov and A. M. Pichugin, Monotonous stability of a conducting fluid advective flow in a weak transverse magnetic field. *Magn. Hydro.*, No. 3, p. 127 (1989).
16. V. M. Myznikov, On decrements spectrum of stationary advective flow of viscous liquid caused by longitudinal temperature gradient. In *Convective Flows and Hydrodynamic Stability*, p. 29. Ural Branch U.S.S.R. Acad. Sci., Sverdlovsk (1979).
17. V. M. Myznikov, On stability of stationary advective liquid flow in plane horizontal layer with free boundary. *Convective Flows. Perm: Pedagog. Inst.*, p. 52 (1979).
18. V. M. Myznikov, On stability of stationary advective flow with respect to spatial disturbances in horizontal layer with free boundary. *Convective Flows. Perm: Pedagog. Inst.*, p. 83 (1981).
19. H. Ben Hadid, B. Roux and P. Laure, Thermocapillary effects on the stability of buoyancy-driven flows in shallow cavities. *PCH* **11,** 625–644 (1989).
20. J. E. Hart, Stability of thin non-rotating Hadley circulations. *J. Atmos. Sci.* **29,** 687–697 (1972).
21. J. E. Hart, A note on the stability of low Prandtl number Hadley circulation. *J. Fluid Mech.* **132,** 271–282 (1983).
22. H. P. Kuo and S. A. Korpela, Stability and finite amplitude natural convection in a shallow cavity with insulated top and bottom and heated from a side. *Phys. Fluids* **31,** 33–42 (1988).
23. V. M. Myznikov, On perturbation form of plane-parallel convective flow in a horizontal layer. *Hydrodynamics. Perm: Pedagog. Inst.*, No. 7, p. 33 (1974).
24. P. Laure and B. Roux, Linear and non-linear analysis of the Hadley circulation. *J. Cryst. Growth* **97,** 226–234 (1989).
25. M. K. Smith and S. H. Davis, Instabilities of dynamic thermocapillary liquid layers. Part 1. Convective instabilities. *J. Fluid Mech.* **132,** 119–144 (1983).
26. M. K. Smith, The nonlinear stability of dynamic thermocapillary liquid layers. *J. Fluid Mech.* **194,** 391–415 (1988).